Journal of Porous Materials
https://doi.org/10.1007/s10934-019-00830-x

Surfactant-assisted imidacloprid intercalation of layered zinc hydroxide nitrate: synthesis, characterisation and controlled release formulation

Sharifah Norain Mohd Sharif[1] · Norhayati Hashim[1,2] · Illyas Md Isa[1,2] · Suriani Abu Bakar[2,3] · Mohamad Idris Saidin[1] · Mohamad Syahrizal Ahmad[1] · Mazidah Mamat[4] · Mohd Zobir Hussein[5]

Abstract
A neutrally charged insecticide, imidacloprid (IC), has been intercalated into zinc hydroxide nitrate (ZHN) with the assistance of sodium dodecylsulphate (SDS). The presence of SDS assists the intercalation of IC by forming a hydrophobic region in the interlayer gallery of ZHN. The intercalated compound, ZHN–SDS–IC, was characterised using powder X-ray diffraction (PXRD), thermogravimetric analysis, Fourier transform infrared spectroscopy, elemental analysis, field emission scanning electron microscopy, and gas sorption analysis. The PXRD studies demonstrated intercalation peaks at lower 2θ, which confirmed the intercalation of IC and SDS in the interlayer gallery of ZHN. The release and kinetic studies of ZHN–SDS–IC reveals that the IC were successfully released in controlled manner (with release time up to 1478 min), and were governed by pseudo second order kinetic model. The ZHN–SDS–IC synthesised is hopefully beneficial in overcoming the consequences of excessive usage of insecticide in paddy cultivation.

Keywords Imidacloprid · Zinc hydroxide nitrate · Intercalation · Sodium dodecylsulphate · Controlled release formulation

1 Introduction

Recently, intense research interests have paid on layered metal hydroxides (LMHs) due to their ability to intercalate various organic molecules in the interlayer gallery [1–7]. LMHs are commonly categorised into layered double hydroxides (LDHs) and layered hydroxide salts (LHSs). Both LDHs and LHSs are types of brucite ($Mg(OH)_2$) structure. LDHs are formed when some of the Mg^{2+} in the brucite structure are replaced with trivalent cations, M^{3+}, thus producing an excess charge on the layer, that needs to be counter balanced by interlayer anions [8]. LHSs are formed when some of the hydroxyl ions in the brucite structure are substituted by water molecules and guest anions [9]. The general formula of LHS structures is $M^{2+}(OH)_{2-x}(A^{m-})_{x/m}{\cdot}nH_2O$, where M^{2+} represents the metal cation and A^{m-} refers to the counter ion [10].

In particular, zinc hydroxide nitrate (ZHN; $Zn_5(OH)_8(NO_3)_2{\cdot}2H_2O$), has drawn considerable attention as a host material for intercalation compounds [8, 9, 11, 12]. Each layer of ZHN is made up of octahedral coordinated zinc cations, with one-quarter of the octahedral sites unoccupied. Positioned above and below the unoccupied octahedral sites are zinc tetrahedra. The water molecules occupy the vertices of the tetrahedral and the nitrate anions in the interlayer gallery are exchangeable [13]. Some of the interesting characteristics own by ZHN is their easy preparation and greater exchange capacity (3.2 meq/g) comparable to LDH [14]. ZHN has been reported to be intercalated with various

✉ Norhayati Hashim
norhayati.hashim@fsmt.upsi.edu.my

1 Department of Chemistry, Faculty of Science and Mathematics, Universiti Pendidikan Sultan Idris, 35900 Tanjong Malim, Perak, Malaysia

2 Nanotechnology Research Centre, Faculty of Science and Mathematics, Universiti Pendidikan Sultan Idris, 35900 Tanjong Malim, Perak, Malaysia

3 Department of Physics, Faculty of Science and Mathematics, Universiti Pendidikan Sultan Idris, 35900 Tanjong Malim, Perak, Malaysia

4 School of Fundamental Science, Universiti Malaysia Terengganu, 21030 Kuala Terengganu, Terengganu, Malaysia

5 Materials Synthesis and Characterization Laboratory, Institute of Advanced Technology, Universiti Putra Malaysia, 43400 Serdang, Selangor, Malaysia

Published online: 21 November 2019

types of guest anions, including metalloporphyrins [15], 2-mercaptobenzoic acid, 2-aminobenzoic acid and 4-aminobenzoic acid [16], oxalatooxoniobate [11], adipate, azelate, and benzoate [12]. Indeed, recent studies have also reported other applications of ZHN, including as a catalyst for the esterification of free fatty acids and the transesterification of vegetable oils [17], and as a starting material in synthesising nickel doped zinc oxide nanoparticles [18].

It has been well-known that one of the unique properties of both LDHs and LHSs is their versatility. These host materials are not only reported to intercalate anionic guest ions, but also poorly water soluble and neutrally charged guest ions. However, the neutral charge guest ion may not be directly intercalated into the interlayer gallery of LDHs and LHSs owing to the neutral charge possessed by this ion. Therefore, the presence of an anionic surfactant such as sodium dodecylsulphate (SDS) or calcium dodecylbenzenesulfonate (CDBS) is necessary to create a hydrophobic region in the interlayer gallery, thus assisting the intercalation process [8, 19]. Several examples of neutral charge ions that were intercalated into LDHs and LHSs with the assistance of surfactants are chlorpyrifos [8], hexaconazole, and triadimenol [19].

Imidacloprid (IC), also known under the IUPAC name of *N*-[1-[(6-chloro-3-pyridyl)methyl]-4,5-dihydroimidazol-2-yl]nitramide, was the earliest commercialised member of a new class of insecticides known as neonicotinoids [20]. The structure of IC is shown in Fig. 1. The physical and chemical properties of IC enable the rapid translocation of residues across the whole of the treated plants. This systemic insecticide acts by disturbing nicotinic acetylcholine receptors in the insect central nervous system. IC is a neutrally charged and poorly water soluble pesticide that was frequently used to deal with various sucking insects such as brown, white-backed, and small brown planthoppers, soil insects, termites, and several chewing insects that were commonly found in paddy cultivation areas. Even though IC can be used to exterminate various pests, its residues however may risk human health once it enters water bodies [21]. Hence, it is important to control the spread of its residues.

The application of the controlled release formulation (CRF) into the pesticides is one of the effective ways to control the spread of the pesticide residues into the environment [22–24]. CRFs are fabricated to shield the supply of the active ingredient, to permit the release of this one to the target at a controlled rate, and to sustain its concentration in the system within the optimal limits over a certain duration, hence providing excellent specificity and perseverance [25]. The development of CRF of IC could be very beneficial for commercial formulations, as the CRF can deliver an enhancement in safety to the community and non-target organisms, by lessen the pesticide application rates and the possibility of leaching in soils [26–29].

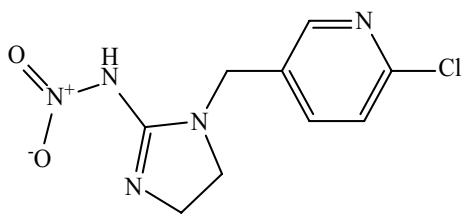

Fig. 1 The chemical structure of imidacloprid (IC)

In this study, IC was selected to be intercalated into the interlayer gallery of ZHN in the presence of the SDS surfactant. The intercalation of IC into the interlayer gallery of Zn/Al–LDH has been recently reported [30] but to the best of our knowledge there have been no reports on the intercalation of IC into the interlayer gallery of ZHN. Further experiments on the potential of a the novel zinc hydroxide nitrate–sodium dodecylsulphate–imidacloprid (ZHN–SDS–IC) nanocomposite synthesised for the sustained release of IC from its interlayer gallery was then investigated using several concentrations of aqueous salt solutions that contained phosphate (PO_4^{3-}), sulphate (SO_4^{2-}) and chloride (Cl^-) as the release media. A study of the synthesis of ZHN-SDS-IC for the purpose of controlled release has not yet been reported.

2 Experimental

2.1 Materials

Both $Zn(NO_3)_2{\cdot}6H_2O$ (purity 98%) and SDS were bought from systerm. The intercalated guest IC was purchased from China (purity 98%). The NaOH and HCl that were used to adjust the pH of the solutions were obtained from Merck and Sigma-Aldrich, respectively. Deionised water was used throughout the study. All reagents were used as received and no further purification was performed.

3 Synthesis of ZHN–SDS–IC nanocomposite

ZHN–SDS–IC nanocomposites were prepared according to the method described in [8]. The ZHN–SDS was initially synthesised by co-precipitation. A 40 mL solution of 0.25 M SDS was prepared and continuously stirred under a constant flow of nitrogen, and a 40 mL solution of 0.5 M $Zn(NO_3)_2{\cdot}6H_2O$ and 1 M NaOH was prepared; both solutions were then simultaneously and slowly added into the $Zn(NO_3)_2{\cdot}6H_2O$ solution. HCl was added dropwise when needed to control the pH to a value of 6.5. The slurry mixture obtained was aged at 70 °C in an oil bath shaker for 24 h and centrifuged at 40 rpm for 5 min to collect the precipitate. The precipitate was oven dried at 60 °C, then ground into a

fine powder. This ZHS–SDS powder was stored in sample bottles.

For the synthesis of the ZHN–SDS–IC nanocomposite, 50 mL of 0.02 M IC solution was prepared by dissolving the IC in dichloromethane and deionised water, with the volume ratio of dichloromethane to deionised water was 1 : 1. The previously prepared ZHN–SDS powder (0.3 g) was dispersed in the IC solution. Deionised water (20 mL) was added into the mixture, which was then stirred for 2 h. The resulting mixture was aged at 70 °C in an oil bath shaker for 24 h. The mixture was centrifuged at 40 rpm for 5 min, oven dried overnight at 60 °C, ground into a fine powder, and then stored in sample bottles. The same procedure was repeated using two further concentrations of IC (0.01 M and 0.005 M).

4 Characterisation

The powder X-ray diffraction (PXRD) equipment used was PANalytical X'pert Pro MPD, using Co Kα radiation (0.15406 nm). The measurements were performed in the range of 2–60° and the measurement conditions were: step size, 0.0330°; scan step time, 19.4434 s; and generator settings, 30 mA, 40 kV. Infrared absorbance was recorded on a Nicolet Fourier transform infrared (FTIR) spectrometer from Thermo Electron Corporation in the range of 400–4000 cm^{-1}. The KBr pellet was prepared using the KBr pellet technique by pressing the samples into KBr discs. The KBr powder containing approximately 1% sample are finely ground and homogenously mixed to ensure the sample is dispersed uniformly in FTIR grade KBr powder. The mixture of KBr and the sample was placed in a press and put under pressure to produce a transparent pellet. The pellet was then placed directly in the infrared beam.Thermogravimetric analyses (TGA) were performed using a Perkin-Elmer Pyris 1 TGA Thermo Balance. The sample were heated from room temperature until 1000 °C, and the heating rate was set to 10 °C min^{-1}. The TGA analysis was ran under environment of nitrogen (flowing at 85 ± 5 ml/min), with sample sizes of 15.0 ± 1.0 mg contained in aluminium sample cups. Carbon, nitrogen, and hydrogen contents were analysed by a CHNS elemental analyser (model CHNS-932 LECO), whereas the metal contents of the samples were determined using inductively coupled plasma optical emission spectrometry (ICP-OES; model Perkin-Elmer Plasma 1000). Field emission scanning electron microscopy (FESEM) images were obtained using a Hitachi SU 8020 UHR instrument whereas the Quantachrome Autosorb automated gas sorption analyser was used for analysis of the surface properties using nitrogen adsorption–desorption techniques. The pore size distribution and the surface area of both materials were evaluated using the Barrett–Joyner–Halenda (BJH) and Brunauer–Emmett–Teller (BET) methods, respectively.

5 Controlled released study of the IC from ZHN–SDS–IC nanocomposite

The controlled released study of IC from the ZHN–SDS–IC nanocomposite was conducted using Perkin Elmer ultraviolet visible (Uv–vis) spectrometer. Deionised water was used as a blank and three types of salt solutions with different concentration were used as release media, which are sodium sulphate (Na_2SO_4), sodium phosphate (Na_3PO_4) and sodium chloride (NaCl). The aqueous solutions for the single system were prepared in 0.1 M, 0.3 M and 0.5 M while the binary and ternary system were prepared in 0.5 M aqueous solutions. 3.5 mL of the salt solutions was placed in a cuvette and 0.6 mg of nanocomposite was then added. The cuvette was closed and covered using parafilm. The cuvette was left for a few days in the Uv–vis spectrometer so that their controlled release behaviour can be observed. The duration for the release process may be varied according to the type of aqueous solution used, which is based on the observation made on the graph generated by the Uv–vis spectrometer (until the curve has reach a plateau). The release study for each nanocomposite was conducted at their respective lambda max using similar experimental conditions of Uv–vis measurements (time interval = 60 s, slit width = 1.0 nm, lamp change = 326.0 nm, ordinate max = 1.0 and ordinate min = 0.0).

6 Results and discussion

6.1 PXRD analysis

PXRD was the preliminary method used to validate whether the layered structure of ZHN–SDS was altered or not after treatment with IC. The validation was made based on the changes observed in the basal spacing after the reaction [11]. The PXRD pattern of the ZHN–SDS showed a basal spacing of 33.0 Å (Fig. 2a), and after intercalation the basal spacing of ZHN–SDS–IC was slightly decreased, to 32.0–32.1 Å (Fig. 2c–e). This decrease in basal spacing may be due to the elimination of some SDS molecules from the interlayer gallery, which go on to form SDS–IC micelles in the solution [8]. Even though the change in the basal spacing was small, the interlayer spacing is large enough to contain both SDS and IC.

The PXRD analyses of the ZHN–SDS–IC nanocomposites also revealed that the concentration of IC significantly affects the appearance of the intercalation peaks. In the PXRD pattern of the ZHN–SDS–IC nanocomposite

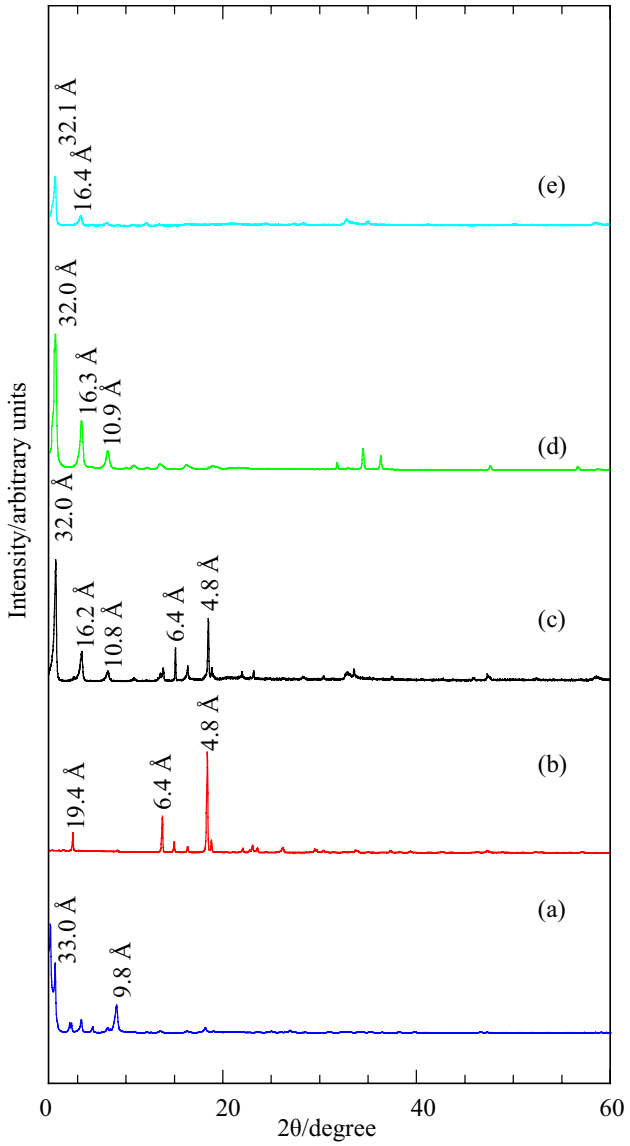

Fig. 2 PXRD patterns of **a** ZHN–SDS and **b** IC; and ZHN–SDS–IC nanocomposites prepared using **c** 0.02 M, **d** 0.01 M, and **e** 0.005 M IC

synthesised using 0.02 M IC, the presence of several peaks that were also found in the PXRD pattern of the IC are noticeable (6.4 and 4.8 Å). These peaks indicate that the amount of IC available during the intercalation reaction is in excess, hence some of the IC remains unreacted. However, as the concentration of IC was reduced to 0.01 M**,** a series of symmetrical, sharp and intense peaks with basal spacing of 32.0, 16.3, and 10.9 Å appeared. The characteristic of these peaks denotes the formation of well-ordered layered structures [31]. The PXRD patterns also reveal that the ZHN–SDS–IC nanocomposite synthesised using 0.01 M IC shows better intensity and crystallinity compared to those with 0.005 M and 0.02 M IC. Further reducing the concentration of IC, however, only led to the diminishment of the intercalation peaks. Moreover, some of the intercalation peaks disappeared when the concentration of IC was reduced to 0.005 M. Hence, the nanocomposite that was synthesised using 0.01 M IC was chosen to be characterised further.

7 Spatial orientation of SDS and IC in the ZHN interlayer

Figure 3 a, b illustrate the three-dimensional size of IC and SDS, respectively, as predicted by Chem 3D Ultra 8.0 software. The x, y, and z axes of IC were determined to be 9.2, 12.5, and 7.3 Å, whereas the x, y, and z axes of SDS were determined to be 6.1, 19.9, and 5.2 Å. Taking into consideration that the thickness of the ZHN layer is 4.8 Å, the thickness of each Zn tetrahedron is 2.6 Å, and the basal spacing of ZHN–SDS–IC is 32.0 Å (as determined by PXRD), the height of the interlayer gallery of ZHN–SDS–IC is calculated to be 22.0 Å. Hence, the intercalated SDS and IC are believed to be in a vertical monolayer arrangement. The spatial orientations of SDS and IC in the interlayer gallery of ZHN were predicted using Chem 3D Ultra 8.0 software, as illustrated in Fig. 3c.

During the intercalation process, the negatively charged functional group of SDS was attracted to the positively charged ZHN layer via electrostatic force, hence creating a hydrophobic region in the interlayer gallery that enabled the intercalation of the poorly water soluble IC [8, 19, 30]. Therefore, it can be proposed that the incorporation of IC into the ZHN–SDS was succeeded in two intercalation steps. A hydrophobic region was first created and the interlayer gallery of ZHN was enlarged during the intercalation of SDS. The intercalation of IC occurred successively in the hydrophobic region of the enlarged gallery during the second intercalation [8]. The suggested mechanism for the reaction is illustrated in Fig. 4.

8 FTIR analysis

The intercalation of IC into the interlayer gallery of ZHN–SDS was further confirmed via FTIR analysis. Figure 5 shows the FTIR spectra of ZHN–SDS (Fig. 5a), IC (Fig. 5b), and the ZHN–SDS–IC nanocomposite (Fig. 5c). A broad peak corresponding to the –OH group stretching vibration in the interlayer gallery and interlayer water molecule can be seen in the FTIR spectra of ZHN–SDS and ZHN–SDS–IC at around 3458 cm^{-1} and 3492 cm^{-1}, respectively [32]. A sharp peak at 3575 cm^{-1} was also observed seen in the FTIR spectra of ZHN–SDS, which can be

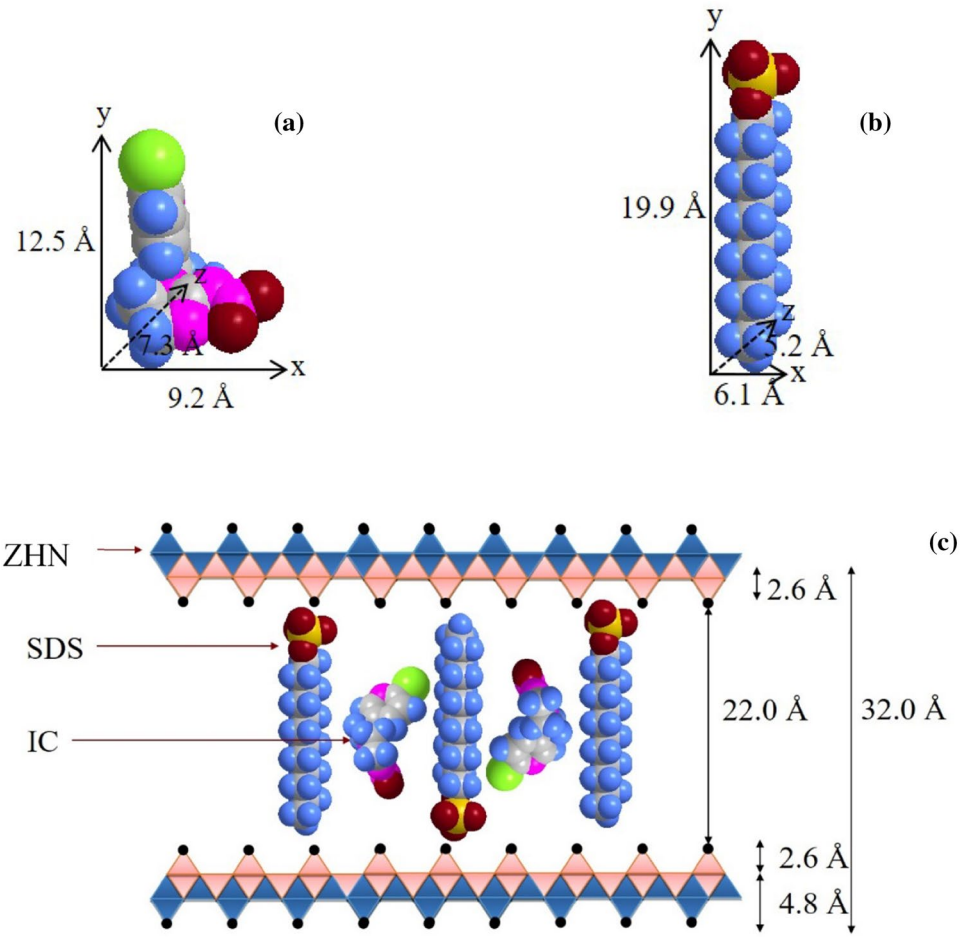

Fig. 3 Three-dimensional molecular structure of **a** imidacloprid and **b** sodium dodecylsulphate, and **c** the spatial orientation of IC and SDS in the interlayer gallery of ZHN–SDS–IC

attributed to the well-defined vibrational energy that comes from the –OH group in the inorganic lattice [8].

The FTIR spectra of ZHN–SDS display several peaks that correspond to the characteristic peaks of SDS such as those at 2957, 2920, and 2848 cm^{-1} for the C–H stretching and bending [33, 34], peaks at 1085 and 1217 cm^{-1} for the symmetric and asymmetric stretching of S=O [30], and a peak at 827 cm^{-1} for the stretching vibration of S–O [8]. Similar characteristic peaks of SDS were also observed in the FTIR spectra of the ZHN–SDS–IC nanocomposite at 2938, 960, and 751 cm^{-1} which result from the C–H, S=O, and S–O stretching, respectively. Hence, this indicates the existence of the SDS molecule in the interlayer gallery of both ZHN–SDS and ZHN–SDS–IC nanocomposite.

There are also a number of peaks that exist in the FTIR spectra of both IC and ZHN–SDS–IC nanocomposite. In the FTIR spectra of IC, the characteristic peaks emerge at 1559, 1388, and 1102 cm^{-1}, which are attributed to pyridine, N–O, and C–Cl stretching vibrations. Similar stretching can be seen in the FTIR spectra of ZHN–SDS–IC in the peaks at 1609, 1431, and 1180 cm^{-1}, respectively. This signifies that the IC were successfully loaded into the ZHN–SDS interlayer gallery.

In summary, the FTIR analyses reveal that certain peaks in the FTIR spectra of both IC and SDS were found in the FTIR spectra of the ZHN–SDS–IC nanocomposite, which indicates the presence of IC and SDS in the interlayer gallery of ZHN. The positions of these peaks, however, may be slightly shifted as a result of the interactions between the IC, SDS, and ZHN after intercalation [35].

9 Elemental analysis

The elemental analysis of ZHN–SDS, IC, and ZHN–SDS–IC nanocomposite obtained from ICP-OES and CHNS analyses are presented in Table 1. Taking the percentage of nitrogen in ZHN–SDS–IC as 11.20%, as determined by CHNS analysis, the percentage loading of IC in the interlayer of ZHN–SDS–IC is calculated to be 40.88%. Based on the elemental analysis and thermogravimetric studies, the chemical formula of ZHN-SDS-IC synthesised can be proposed as $Zn(OH)_{1.89}(CH_3(CH_2)_{11}SO_4)_{0.12}(C_9H_{10}ClN_5O_2)_{0.43}.0.76\ H_2O$. The results obtained from the elemental analysis, are therefore, validate the successful intercalation of IC into the interlayer gallery of the ZHN–SDS host.

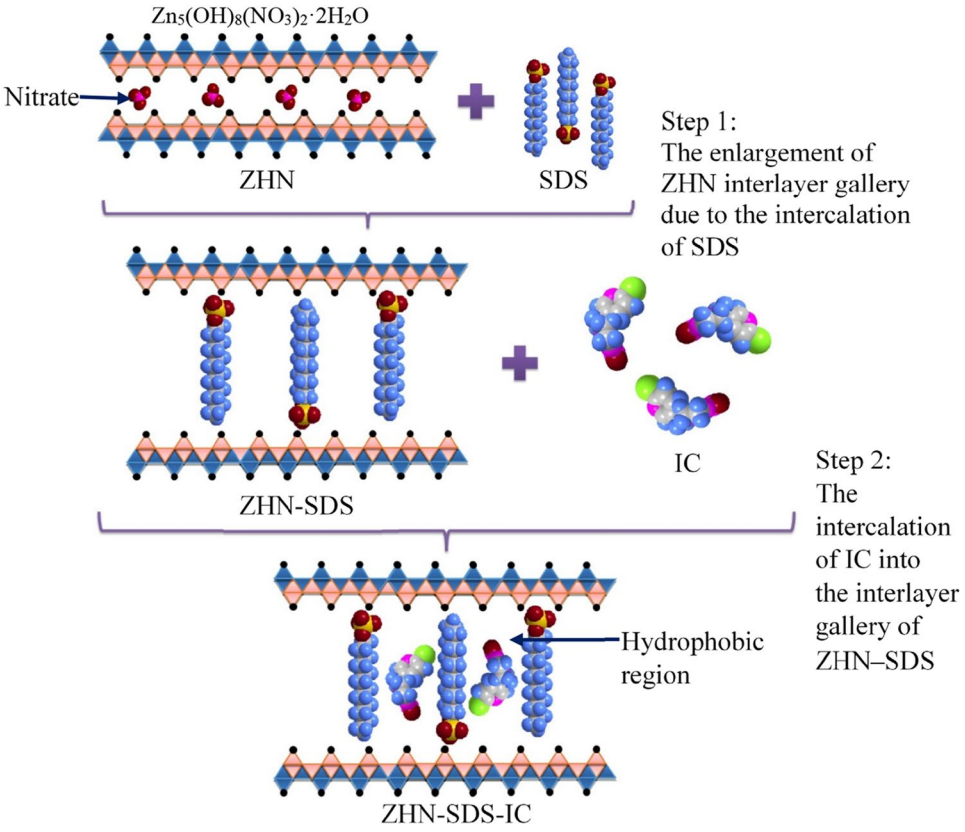

Fig. 4 The intercalation mechanism of the ZHN–SDS–IC nanocomposite

10 Thermal studies

The ZHN–SDS, pristine IC, and ZHN–SDS–IC nanocomposite were analysed by TGA to determine their degradation temperature. The thermal decomposition was observed from 35 to 900 °C. The TGA curve of ZHN–SDS (Fig. 6a) showed two weight loss events, which occurred at 107.1 and 198.2 °C. The first weight loss (of 3.2%) is due to the removal of surface water and structural water, whereas the second weight loss (of 37.2%) corresponds to the dehydroxylation of the lattice together with the decomposition of SDS [13, 34]. The TGA curve of the pristine IC shows the occurrence of one major weight loss at 324.3 °C, which results from the complete thermal decomposition of IC (Fig. 6b).

The ZHN–SDS–IC nanocomposite exhibits four weight loss stages (Fig. 6c). The first thermal decomposition (at 108.1 °C with 6.2% weight loss) corresponds to the removal of adsorbed and structural water molecules; the second thermal event (at 166.4 °C with 31.2% weight loss) is due to the combustion of organic moieties that come from IC; the third weight loss stage (at 264.2 °C with 3.3% weight loss) is attributed to the decomposition of SDS; and in the fourth stage, part of the layered structure collapsed (at 595.2 °C with 14.3% weight loss) [8, 34, 36].

Based on the results obtained from the thermal studies, it can be seen that the final thermal decomposition of the ZHN–SDS–IC nanocomposite occurred at 595.2 °C, whereas the pristine IC completely decomposed at 324.3 °C, revealing that the ZHN–SDS–IC nanocomposite has better thermal stability than the pristine IC.

11 Surface morphology analysis

FESEM was used to analyse the surface morphology of ZHN–SDS and ZHN–SDS–IC nanocomposite. The images obtained are shown in Fig. 7 a, b, respectively. The results reveal that the surface morphologies of ZHN–SDS and ZHN–SDS–IC nanocomposite are different. The ZHN–SDS demonstrates a non-porous, tabular, stacked plate-like structure with sharp edges; however, this structure was transformed into a thin plate-like structure with more rounded and wrinkly edges as the ZHN–SDS–IC nanocomposite was formed. Although the morphology of both ZHN–SDS and ZHN–SDS–IC are quite different, both still preserve a resemblance to thin lamellar flake-like sheet structures, as predicted for a layered material [37]. Based on the results obtained, it is obvious that the intercalation of IC into the host ZHN–SDS does alter the surface morphology.

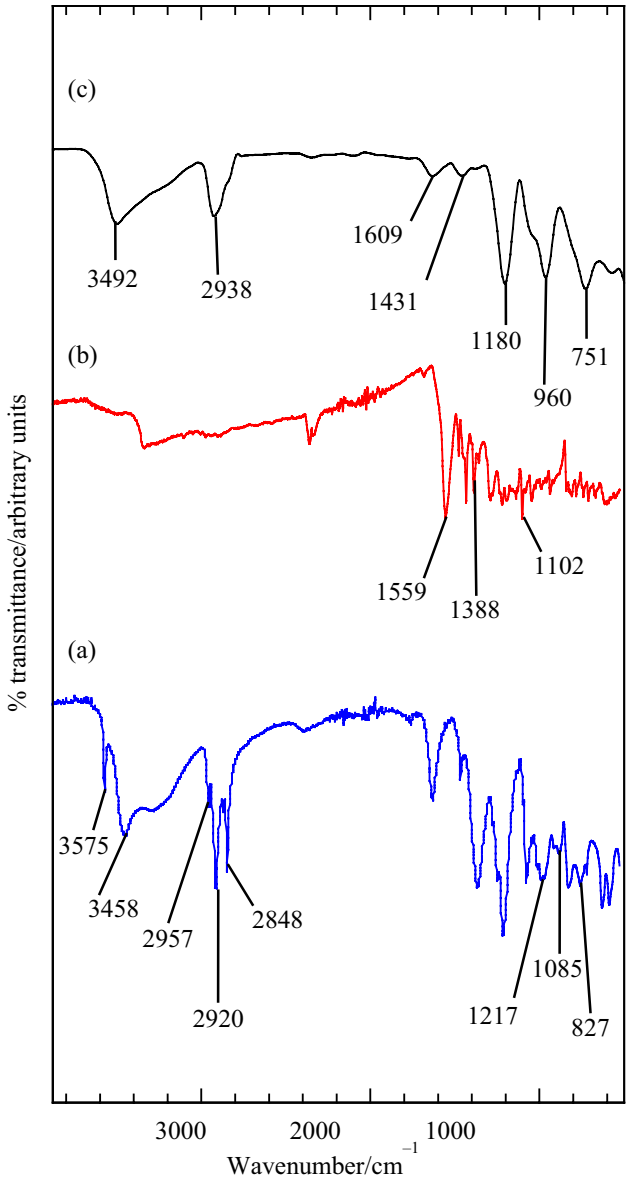

Fig. 5 FTIR spectra of **a** ZHN–SDS **b** IC, and **c** ZHN–SDS–IC nanocomposite

12 Surface properties analysis

The adsorption–desorption isotherms of nitrogen gas and Barrett–Joyner–Halenda (BJH) desorption pore size distributions for ZHN–SDS and ZHN–SDS–IC nanocomposites were shown in Fig. 8. The nitrogen adsorption–desorption isotherm curves of both ZHN–SDS and ZHN–SDS–IC demonstrate characteristics of Type IV materials according to IUPAC classification, i.e. mesoporous solids which show hysteresis loops in their isotherms (Fig. 8a, b) [38, 39]. The H_3 type of hysteresis loop indicates that ZHN–SDS and ZHN–SDS–IC have plate-like particles and slit-shaped pores [40]. The width of the hysteresis loop of the ZHN–SDS–IC nanocomposite is far narrower than that of ZHN–SDS, which indicates that the pore texture changes after intercalation [41]. The adsorption of nitrogen occurs slowly at low relative pressures for both ZHN–SDS and ZHN–SDS–IC nanocomposite. However, it increases rapidly at relative pressures above 0.55 for ZHN–SDS until optimum adsorption was finally achieved at 32 $cm^3\ g^{-1}$. ZHN–SDS–IC saw abrupt adsorption occurring at relative pressures higher than 0.8 until optimum adsorption was achieved at 15.5 $cm^3\ g^{-1}$.

The pore size distribution was evaluated using the BJH method and the results obtained are illustrated in Fig. 8c, d. Two obvious peaks were observed at 1.4 and 7.6 nm in the pore size distribution curve of ZHN–SDS. For ZHN–SDS–IC, three sharp peaks were observed, which centred around 2.3, 3.8, and 9.6 nm. The BJH average pore diameter of ZHN–SDS was determined to be 27.830 nm, which seems to decrease to 22.260 nm after forming ZHN–SDS–IC. Similarly, the total pore volume also reduced from around 0.049 to 0.024 $cm^3\ g^{-1}$ after intercalation. The surface area of both materials were evaluated according to the BET method, and the results show that the surface area of ZHN–SDS was determined to decrease after intercalation to ZHN–SDS–IC, from 7.027 to 4.270 $m^2\ g^{-1}$. The reduction of surface area and pore volume is probably due to the pore blockage that happened after intercalation [42]. The obtained surface properties of ZHN–SDS and ZHN–SDS–IC are tabulated in Table 2.

Table 1 Elemental chemical composition of ZHN–SDS, IC and ZHN–SDS–IC nanocomposite

Sample	Zn (%)	C (%)	H (%)	N (%)	S (%)	IC [a] (%w/w)	[b]Formula
ZHN–SDS	24.14	24.80	5.48	2.46	3.38	–	$Zn(OH)_{1.24}(CH_3(CH_2)_{11}SO_4)_{0.29}(NO_3)_{0.48}.\ 0.40H_2O$
IC	–	41.46	3.81	24.00	0.00	–	$C_9H_{10}ClN_5O_2$
ZHN–SDS–IC	24.05	39.42	3.14	11.20	1.36	40.88	$Zn(OH)_{1.89}(CH_3(CH_2)_{11}SO_4)_{0.12}(C_9H_{10}ClN_5O_2)_{0.43}.\ 0.76H_2O$

[a]Estimated from the percentage of nitrogen obtained from CHNS analysis

[b]Estimated from the ICP–OES, CHNS and TGA/DTG analysis

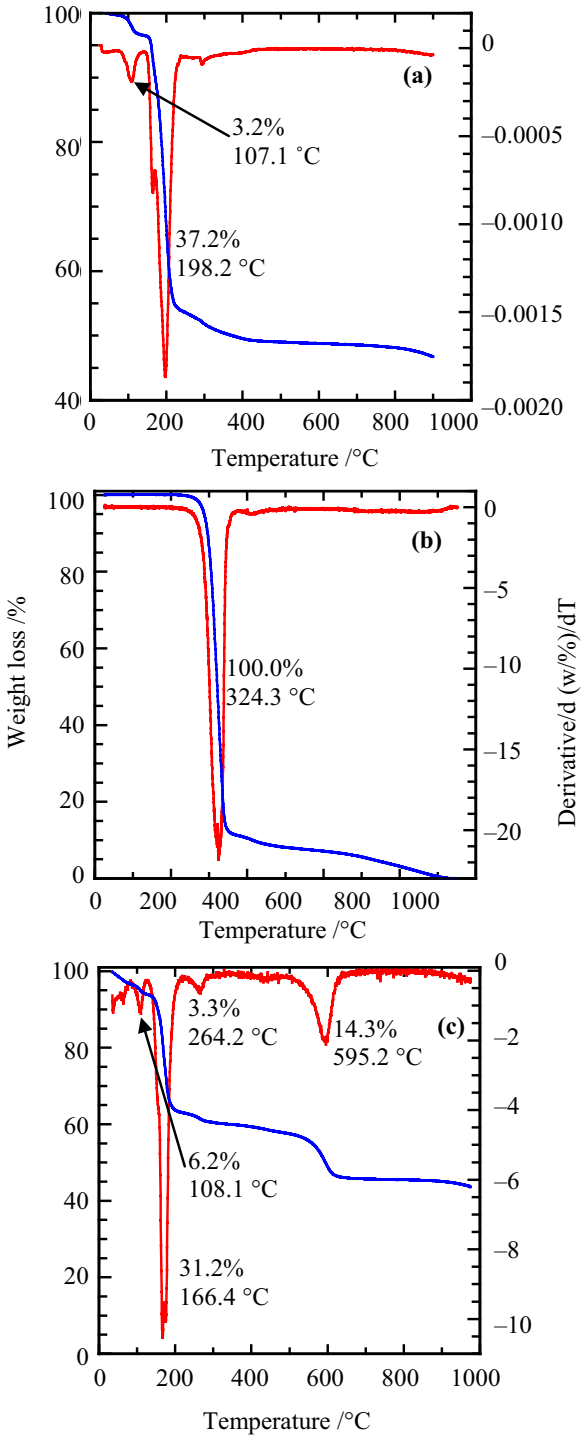

Fig. 6 TGA/DTG curves of **a** ZHN–SDS **b** IC, and **c** ZHN–SDS–IC nanocomposite

The surface properties analyses revealed that the intercalation of IC into the interlayer gallery of ZHN–SDS slightly changes the surface area and porosity of the materials. The surface properties are given in Table 2.

13 Release study of ZHN-SDS-IC nanocomposite into various aqueous solutions

The release of IC from the interlayer gallery of the ZHN–SDS–IC nanocomposite was performed in a release media that consisted single, binary and ternary system of aqueous solutions that contained PO_4^{3-}, SO_4^{2-} and Cl^- anions. This was done because IC is a type of insecticide that is typically used in paddy cultivation areas, and the PO_4^{3-}, SO_4^{2-} and Cl^- supplied by the aqueous solutions are the types of anions that would be commonly available in those areas. In the single system of aqueous solutions, the aqueous solutions of Na_3PO_4, Na_2SO_4 and NaCl were prepared in three different concentrations, namely 0.1 M, 0.3 M and 0.5 M. As for the binary and ternary system, the mixtures were prepared in 0.5 M. The release profiles that correspond to the different types and concentrations of the release media for the release study are shown in Fig. 9.

Based on the release profiles, it can be seen that the ZHN–SDS–IC of IC exhibited slow release properties when the ZHN–SDS–IC nanocomposite was released into the aqueous solutions. In the single system of aqueous solution, the longest release time was when the aqueous solution of NaCl was used as the release media. The time taken for the release decreased in the order as $Cl^- > SO_4^{2-} > PO_4^{3-}$. The result from the release study indicates that the time taken to release IC from the interlayer gallery of ZHN–SDS–IC was greatly affected by the charge density of the aqueous solution. Monovalent Cl^-, which has the lowest charge density compared to the anions provided by other aqueous solutions (SO_4^{2-} and PO_4^{3-}), triggered the occurrence of a slower exchange process between the intercalated IC and the anions available in the aqueous solutions. Hence, it increased the time taken for the release process. A comparable release trend was also reported in a previous study [43–45].

Conducting the release study in aqueous solutions with different concentrations showed an appreciable difference in the time it took for the release. The release of the IC from the interlayer gallery of the ZHN–SDS–IC nanocomposite in 1478 min (0.1 M), 793 min (0.3 M) and 549 min (0.5 M) aqueous NaCl. For the release using aqueous Na_2SO_4 as the release media, the release occurred in 689 min (0.1 M), 473 min (0.3 M) and 302 min (0.5 M). When the aqueous Na_3PO_4 was used as the release media, the release occurred in 310 min (0.1 M), 173 min (0.3 M) and 83 min (0.5 M). Increasing the concentration of the release media accelerated the release process because more anions were present in the release media at a higher concentration [46].

The release studies demonstrated that the release trend for the IC from the interlayer gallery of the ZHN–SDS–IC nanocomposite in each release media seemed to be comparable

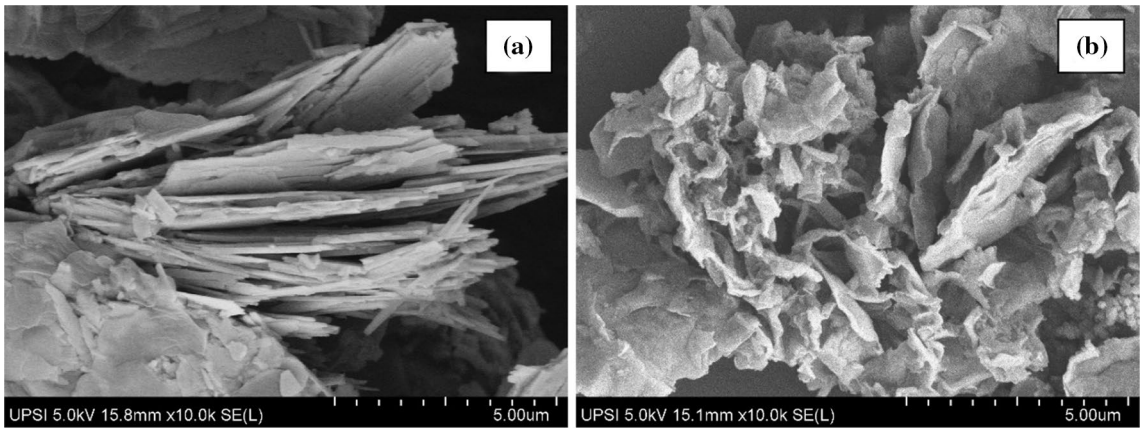

Fig. 7 Surface morphology of **a** ZHN–SDS and **b** ZHN–SDS–IC nanocomposite

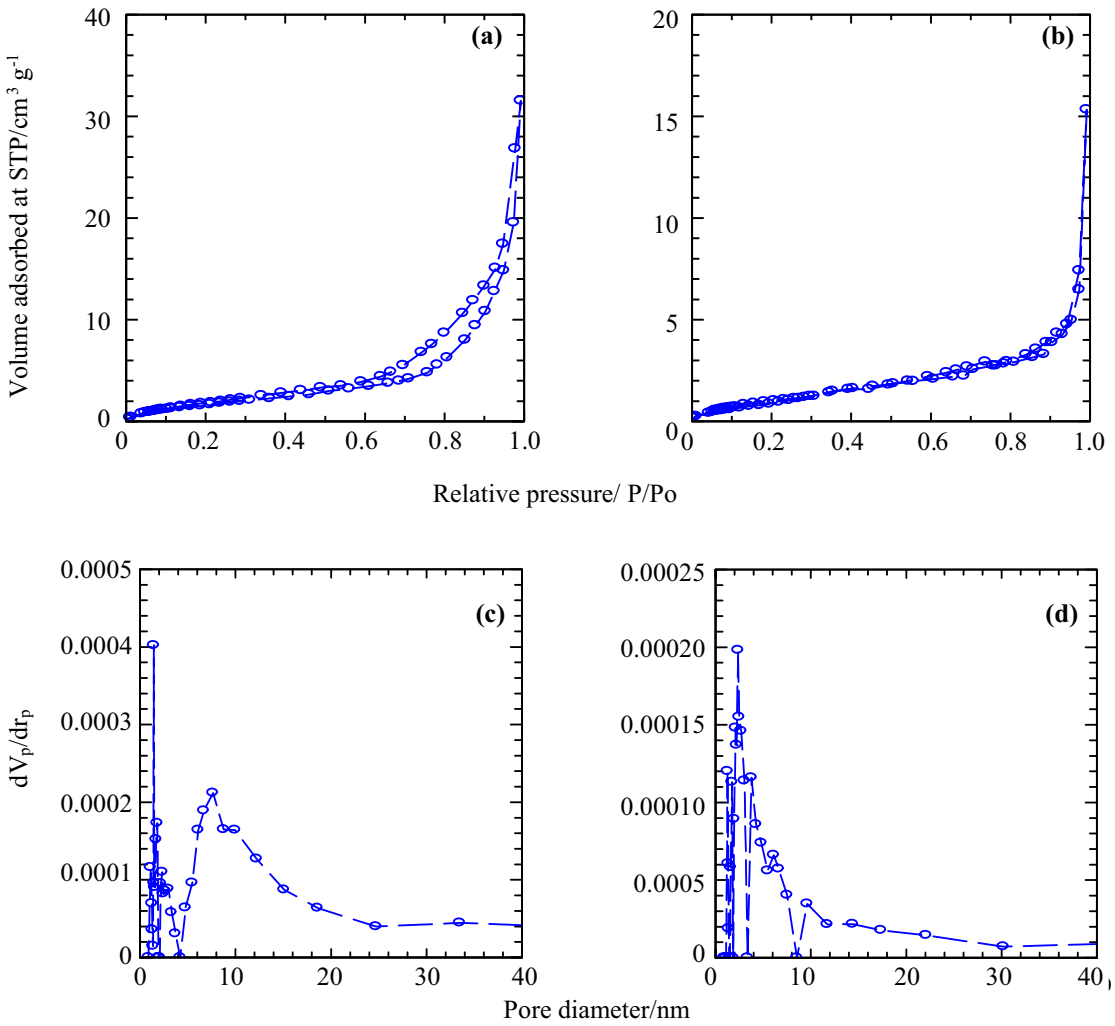

Fig. 8 Adsorption–desorption isotherms of nitrogen gas for **a** ZHN–SDS and **b** ZHN–SDS–IC nanocomposites and Barrett–Joyner–Halenda (BJH) desorption pore size distributions for **c** ZHN–SDS and **d** ZHN–SDS–IC nanocomposites

Table 2 Surface properties of ZHN–SDS and ZHN–SDS–IC nanocomposite

Sample	Basal spacing (Å)	Total pore volume ($cm^3\ g^{-1}$)	Multipoint BET[a] surface area ($m^2\ g^{-1}$)	BJH[b] average pore diameter (nm)
ZHN–SDS	33.0	0.049	7.027	27.830
ZHN–SDS–IC	32.0	0.024	4.270	22.260

[a]Brunauer–Emmett–Teller

[b]Barrett–Joyner–Halenda

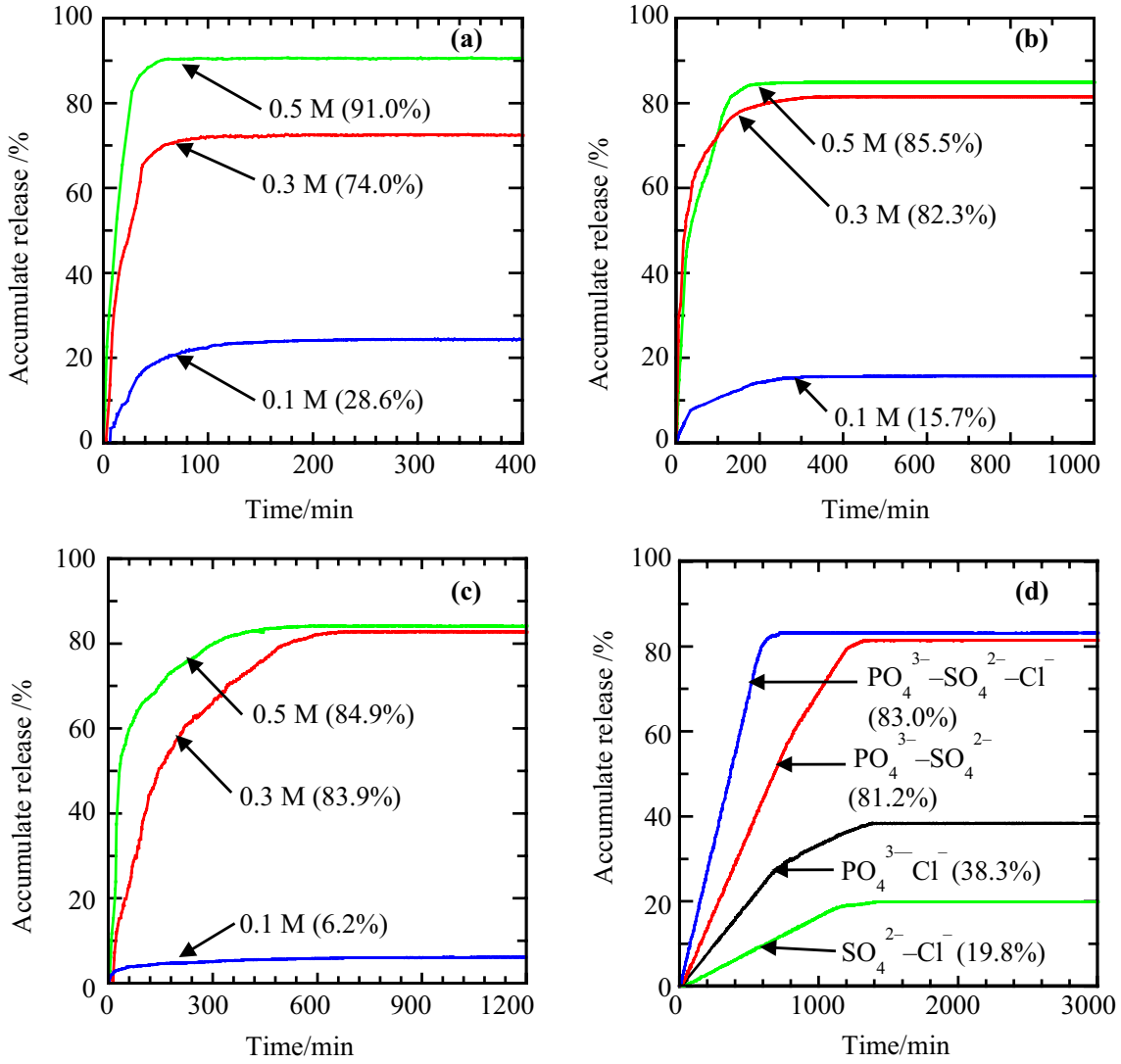

Fig. 9 Release Profiles of IC from ZHN–SDS–IC into aqueous solutions of **a** sodium phosphate, **b** sodium sulphate, **c** sodium chloride and **d** phosphate, sulphate and chloride mixture

and can generally be described as a two–step biphasic process. This was revealed by the occurrence of a burst at the beginning of the release process followed by a slower and more sustained process until the release equilibrium was reached. The abrupt release at the early stage of the release process, which is also known as a burst release phenomenon, may have been triggered by the release of the IC that was adsorbed on the surface of the ZHN–SDS–IC. A higher dissolution rate near the surface of the ZHN–SDS–IC resulted in a higher amount of IC that was released, which triggered the occurrence of the burst release. A similar phenomenon was also reported in recent studies [30, 47].

The results obtained from the release study of ZHN–SDS–IC nanocomposites may also be interpreted in terms of their accumulated percentage release. Releasing the ZHN–SDS–IC nanocomposite in the aqueous Na_3PO_4 permitted the nanocomposite to release 28.6% (0.1 M), 74.0% (0.3 M) and 91.0% (0.5 M) of the intercalated IC in the aqueous Na_3PO_4. The release of ZHN–SDS–IC nanocomposite in the aqueous Na_2SO_4 allowed the release of 15.7% (0.1 M), 82.3% (0.3 M) and 85.5% (0.5 M) of intercalated IC, whereas when the release of ZHN–SDS–IC was performed in aqueous NaCl, 6.2% (0.1 M), 83.9% (0.3 M) and 84.9% (0.5 M) were released.

Even though the intercalated IC was not completely exchanged with the anions that were present in the release media, the accumulated percentage release of the IC was quite high when the ZHN–SDS–IC was released in higher concentrations of aqueous solutions. The accumulated percentage release was in the range of 84.9–91.0% when the release study was performed in 0.5 M aqueous solution. The highest percentage was reached when Na_3PO_4 was used as the release media. The accumulated percentage release of the IC from the interlayer gallery of the ZHN–SDS–IC nanocomposite into the release media was generally in the sequence of $Na_3PO_4 > Na_2SO_4 > NaCl$. A higher accumulated percentage release of the ZHN–SDS–IC nanocomposite occurred in the aqueous Na_3PO_4 because the PO_4^{3-} anions are trivalent and have a higher affinity towards the positively charged ZHN layer than the SO_4^{2-} and Cl^-. This caused the PO_4^{3-} to be more attracted to the ZHN and have a higher tendency to replace the IC that were intercalated in the interlayer gallery of the ZHN–SDS–IC.

The results obtained from the release study of IC from the ZHN–SDS–IC nanocomposite into aqueous solutions of binary and ternary systems of PO_4^{3-}–SO_4^{2-}–Cl^- show that the presence of multiple ions does cause some changes in the release behaviour of IC from the interlayer gallery of ZHN–SDS–IC. In the aqueous solution of the ternary system, the presence of all three anions, PO_4^{3-}–SO_4^{2-}–Cl^-, allows 83.0% of intercalated IC to be released into the release media within 716 min. The release of IC in the ternary system was found to be the highest and the fastest amongst all release media of multiple anion systems. The release of IC in the binary anion system of PO_4^{3-}–SO_4^{2-} was also observed to be significantly high, with 81.2% of accumulated release, and was completed in 1320 min. Although the accumulated release in an aqueous solution of PO_4^{3-}–SO_4^{2-} was slightly lower than the release in the aqueous solution of PO_4^{3-}–SO_4^{2-}–Cl^-, this accumulated release is yet to be the highest of all the release in the binary system. As for the release of IC in the aqueous solutions of PO_4^{3-}–Cl^- and SO_4^{2-}–Cl^-, 38.3% and 19.8% of intercalated IC was released from the interlayer gallery of ZHN–SDS–IC in 1378 min and 1426 min, respectively.

Based on these results, it was observed that a high percentage of accumulated release of IC was obtained in the aqueous solutions involving PO_4^{3-} anions. Therefore, it can be deduced that the fact that PO_4^{3-} possesses a higher affinity towards the positively charged layer of ZHN-SDS compared to both SO_4^{2-} and Cl^- significantly encourages the release process of IC. The presence of Cl^- in the mixture of aqueous solution does, however, decelerate the release process and lower the percentage of accumulated release of IC. This observation was obviously demonstrated by the slowest release process for the aqueous solution of SO_4^{2-}–Cl^- as the release media, with the release process having the slowest rate.

14 Kinetic study of ZHN–SDS–IC into various aqueous solutions

There are several kinetic models that can be used to describe the release process. In this study, five kinetic models were selected for the kinetics analysis. The release data were fitted into zeroth order (Eq. (1)), first-order (Eq. (2)) [48], pseudo-second order (Eq. (3)) [49], parabolic diffusion (Eq. (4)) [50] and Fickian diffusion models (Eq. (5)) [51]. In the zeroth order, the release rate was constant and controlled by polymer relaxation [52]. The intercalated ions were consistently released in a steady state over a fixed time. Based on the first-order kinetic model, the dissolution that occurred in the release process relied on the compounds that were intercalated in the interlayer gallery of the nanocomposite [8]. This kinetic model demonstrated a considerably slower and more variable release rate over time [52]. In the pseudo-second order kinetic model, the release occurred via a diffusion and ion exchange process and was affected by the adsorption factor, liquid film diffusion, surface adsorption and particle inner diffusion. The parabolic diffusion model generally describes the diffusion-controlled process in clays [8]. The Fickian model indicated that the release was diffusion-controlled and the release process proceeded from higher to lower concentration [52]. The equations for each of the kinetics models are as follows:

$$x = t + c \tag{1}$$

$$-\log(1 - M_i/M_f) = t + c \tag{2}$$

$$t/M_i = 1/M_f^2 + t/M_f \tag{3}$$

$$M_i/M_f = kt^{0.5} + c \tag{4}$$

$$M_i/M_f = kt^n \tag{5}$$

where x refers to the percentage release of IC from the interlayer gallery of ZHN-SDS-IC nanocomposite at time, *t; c* is

a constant; k is the rate constant; M_i is the initial concentration of the IC and M_f is the final concentration of the IC in the release media. On the basis of the five kinetics models, the r^2 and k values obtained for the all kinetic models are summarised in Table 3 and the kinetic model that demonstrate the best fit for the release data is shown in Fig. 10.

The curves show that the pseudo second order model better describes the kinetic release process of IC from the interlayer gallery of the ZHN–SDS–IC nanocomposite. The plot of t/M_i vs. time generated fairly straight lines for the pseudo second order model with correlation coefficient, r^2, in the range of 0.958–1.00. The pseudo second order kinetic model that was followed by the ZHN–SDS–IC nanocomposite indicated that the release of the IC from the interlayer gallery of the ZHN–SDS–IC nanocomposite happened through the dissolution of the nanocomposite and the ion exchange process [53]. Considering the type of anions that were available during the release process, it can be proposed that the ion exchange process is actually occurring between the SDS (anionic surfactant) and the incoming anion present in the aqueous solution (PO_4^{3-}, SO_4^{2-} and Cl^-). However, since the intercalated IC is a neutral charge pesticide, the IC is therefore, is capable of forming micelles with the SDS surfactant (SDS-IC micelles) [8]. Hence, allowing the IC to be released into the solution together with SDS.

Fitting the release data into other kinetic models gave poor r^2 values (Table 3). The r^2 values for the release data fit with the zero order model were in the range of 0.185–0.460, first order values were in the range of 0.220–0.540, parabolic diffusion values were in the range of 0.336–0.685 and Fickian diffusion values were in the range of 0.513–0.881.

Noticeable changes in the $t_{1/2}$ value, i.e. the time required for the ZHN–SDS–IC nanocomposite to achieve half of the maximum accumulate release, can be observed in the Table 3. The $t_{1/2}$ is generally higher when the ZHN–SDS–IC was released in the aqueous NaCl and decreased in the order of $Cl^- > SO_4^{2-} > PO_4^{3-}$. A lower affinity for the monovalent Cl^- towards the ZHN layer slowed the exchange process between the intercalated IC and the Cl^- and increased the $t_{1/2}$ values. The $t_{1/2}$ values for 0.1 M NaCl as the release media slightly deviated from this trend due to the low accumulated percentage release obtained (6.2%), which caused the $t_{1/2}$ value to be greatly impacted by the burst release phenomenon. The aqueous solution with higher concentration seemed to have a smaller $t_{1/2}$ due to the fact that more ions were available in the higher concentration of aqueous solution, therefore increasing the rate of the release process [53].

15 Conclusion

ZHN–SDS–IC nanocomposites were successfully synthesised by intercalating IC molecules into the interlayer gallery of ZHN with the assistance of a common surfactant, SDS. The results obtained from the characterisation studies validated the presence of SDS and IC in the interlayer gallery and demonstrated that the synthesised nanocomposite possesses better thermal stability compared to pristine IC. The nitrogen adsorption–desorption isotherm curves of both ZHN–SDS and ZHN–SDS–IC show features of Type IV materials, thus indicating that the materials were made up of mesoporous solids and showed hysteresis loops. The controlled release and kinetic studies reveal the potential of the ZHN–SDS–IC nanocomposite in sustaining the release of IC, and the release of IC from the ZHN–SDS–IC nanocomposites were governed by the pseudo second order model. The highest percentage of the accumulated release was observed when the ZHN–SDS–IC nanocomposites was immersed in the aqueous solutions of Na_3PO_4, in the order of $Na_3PO_4 > Na_2SO_4 > NaCl$, and the slowest release process was observed when the NaCl was used as the release media. To conclude, this study has shown that ZHN is a great host material for intercalation of the poorly

Table 3 Comparison of rate constants (k), regression values (r^2) and half–life ($t_{1/2}$) obtained from the fitting of the release data from ZHN–SDS–IC into aqueous solutions of Na_3PO_4, Na_2SO_4 and NaCl

Aqueous solution		Zero order	First order	Parabolic diffusion	Fickian diffusion	Pseudo second order		
		r^2	r^2	r^2	r^2	r^2	k ($\times 10^{-3}$ s^{-1})	$t_{1/2}$
Na_3PO_4	0.1 M	0.340	0.364	0.551	0.745	1.00	0.448	28.1
	0.3 M	0.238	0.293	0.405	0.553	1.00	0.899	14.0
	0.5 M	0.185	0.220	0.336	0.583	1.00	1.339	9.4
Na_2SO_4	0.1 M	0.316	0.328	0.628	0.837	1.00	0.380	33.1
	0.3 M	0.200	0.279	0.444	0.667	1.00	0.572	22.0
	0.5 M	0.262	0.321	0.472	0.633	1.00	0.812	15.5
NaCl	0.1 M	0.375	0.380	0.685	0.881	1.00	0.546	22.7
	0.3 M	0.460	0.540	0.650	0.573	0.958	0.114	110.5
	0.5 M	0.231	0.394	0.427	0.513	1.000	0.463	27.2

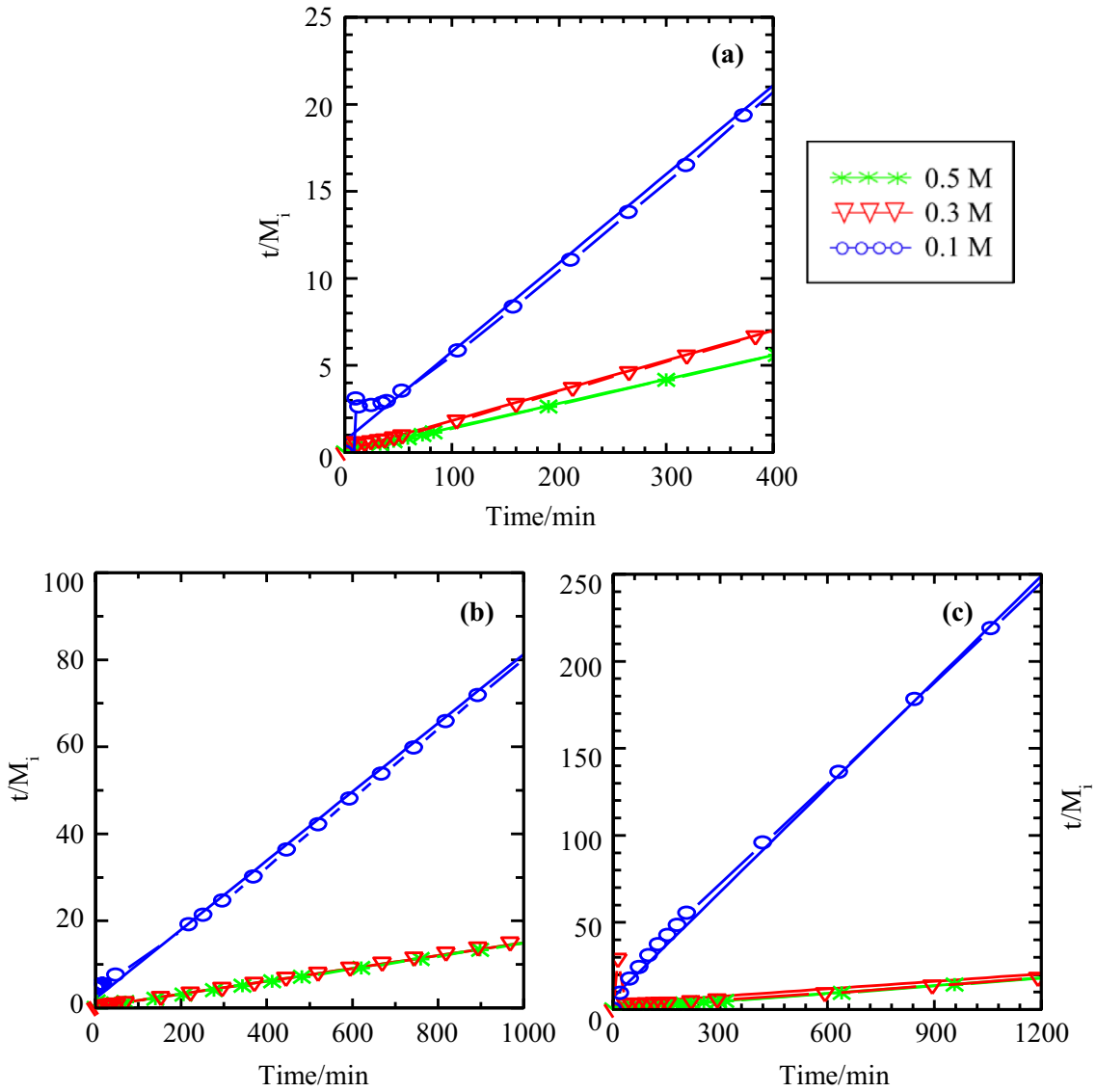

Fig. 10 Fitting of the data for IC release from ZHN–SDS–IC into aqueous solution of **a** sodium phosphate, **b** sodium sulphate and **c** sodium chloride for the pseudo second order kinetic models

water soluble and neutrally charged IC molecule, and the presence of SDS is significantly beneficial for intercalation. The results suggest that the use of ZHN as host materials may be useful in retarding the release of IC pesticides after soil application in paddy cultivation areas.

Acknowledgements The authors wish to thank UPSI and the Ministry of Education Malaysia for supporting this research. This work was supported by the GPU-RISING STAR Grant No. 2019 – 0119 – 103 – 01.

References

1. P. Li, F. Lv, Z. Xu, G. Qi, Y. Zhang, J. Mater. Sci. **48**, 5437 (2013)
2. N. Hashim, S.N.M. Sharif, I.M. Isa, S.A. Hamid, M.Z. Hussein, S.A. Bakar, M. Mamat, J. Phys. Chem. Solids **105**, 35 (2017)
3. Z. Sun, L. Jin, W. Shi, M. Wei, X. Duan, Chem. Eng. J. **161**, 293 (2010)
4. M.Y. Ghotbi, M.Z. Hussein, J. Phys. Chem. Solids **71**, 1565 (2010)
5. W.G. Hou, Z.L. Jin, Colloid Polym. Sci. **285**, 1449 (2007)
6. L. Moyo, W.W. Focke, F.J.W.J. Labuschagne, S. Verryn, Mol. Cryst. Liq. Cryst. **555**, 51 (2012)
7. R. Marangoni, A. Mikowski, F. Wypych, J. Colloid Interface Sci. **351**, 384 (2010)
8. J. Liu, X. Zhang, Y. Zhang, A.C.S. Appl, Mater. Interfaces **7**, 11180 (2015)
9. S. Jaerger, A. Zimmermann, S.F. Zawadzki, F. Wypych, S.C. Amico, Polimeros **24**, 683 (2014)
10. F.M. Fernandes, H. Baradari, C. Sanchez, Appl. Clay Sci. **100**, 2 (2014)

11. G. G. C. Arizaga, J. E. F. Da Costa Gardolinski, W. H. Schreiner, F. Wypych, J. Colloid Interface Sci. **330**, 352 (2009).
12. G. G. C. Arizaga, A. S. Mangrich, J. E. F. da Costa Gardolinski, F. Wypych, J. Colloid Interface Sci. **320**, 168 (2008).
13. H.S. Bae, H. Jung, Bull. Korean Chem. Soc. **33**, 1949 (2012)
14. J. Demel, P. Kubát, I. Jirka, P. Kovář, M. Pospíšil, K. Lang, J. Phys. Chem. C **114**, 16321 (2010)
15. G. S. Mac Hado, G. G. C. Arízaga, F. Wypych, S. Nakagaki, J. Catal. **274**, 130 (2010).
16. A.C.T. Cursino, J.E.F.C. Gardolinski, F. Wypych, J Colloid Interface Sci. **347**, 49 (2010)
17. C.S. Cordeiro, G.G.C. Arizaga, L.P. Ramos, F. Wypych, Catal. Commun. **9**, 2140 (2008)
18. M.Y. Ghotbi, Particuology **10**, 492 (2012)
19. Q. Zhenlan, Y. Heng, Z. Bin, H. Wanguo, Colloids Surfaces A Physicochem. Eng. Asp. **348**, 164 (2009)
20. I. Ishaaya, A. R. Horowitz, in *Insectic. with Nov. Modes Action*, ed. by I. Ishaaya, D. Degheele (Springer, Berlin, Heidelberg, 1998), pp. 1–24
21. J.E. Jepson, L.A. Brown, D.B. Sattelle, Invert Neurosci. **6**, 33 (2006)
22. A. Nennemann, Y. Mishael, S. Nir, B. Rubin, H. Van Damme, G. Lagaly, (2001).
23. A.M. Bashi, M.Z. Hussein, Z. Zainal, M. Rahmani, D. Tichit, Arab. J. Chem. **9**, 1457 (2016)
24. X. Zhang, J. Liu, W. Hou, J. Tong, L. Ren, G. Sun, Y. Sun, (2016).
25. F.F. Céspedes, S.P. García, M.V. Sánchez, M.F. Pérez, Chemosphere **92**, 918 (2013)
26. R. Celis, M.C. Hermosín, L. Cornejo, M.J. Carrizosa, J. Cornejo, Int. J. Environ. Anal. Chem. **82**, 503 (2002)
27. J. Li, J. Yao, Y. Li, Y. Shao, J. Environ. Sci. Heal. **47**, 795 (2012)
28. S. Bakhtiary, M. Shirvani, H. Shariatmadari, Chemosphere **90**, 699 (2013)
29. B. Azeem, K. Kushaari, Z.B. Man, A. Basit, T.H. Thanh, J. Control. Release **181**, 11 (2014)
30. D.P. Qiu, W.G. Hou, J. Xu, J. Liu, S. Liu, Chinese J. Chem. **27**, 1879 (2009)
31. Q. Chen, S. Shi, X. Liu, L. Jin, M. Wei, Chem. Eng. J. **153**, 175 (2009)
32. A.A. Al-Kahtani, B.S. Sherigara, Carbohydr. Polym. **104**, 151 (2014)
33. M. Li, S. Chen, F. Ni, Y. Wang, L. Wang, Electrochim. Acta **53**, 7255 (2008)
34. Q. Tao, J. Yuan, R.L. Frost, H. He, P. Yuan, J. Zhu, Appl. Clay Sci. **45**, 262 (2009)
35. M.Z. Hussein, N.F. Nazarudin, S.H. Sarijo, M.A. Yarmo, J. Nanomater. **2012**, 1 (2012)
36. Q. Li, M. Meng, Z.Q. Zou, X.G. Li, Y.Q. Zha, J. Hazard. Mater. **161**, 366 (2009)
37. G.G.C. Arizaga, K.G. Satyanarayana, F. Wypych, Solid State Ionics **178**, 1143 (2007)
38. J.S. Valente, F. Tzompantzi, J. Prince, Appl. Catal. B Environ. **102**, 276 (2011)
39. H. Nabipour, M. Hosaini Sadr, N. Thomas, M. H. Sadr, N. Thomas, J. Exp. Nanosci. **10**, 1269 (2015).
40. C. Geng, T. Xu, Y. Li, Z. Chang, X. Sun, X. Lei, Chem. Eng. J. **232**, 510 (2013)
41. S.A.I.S.M. Ghazali, M.Z. Hussein, S.H. Sarijo, Nanoscale Res. Lett. **8**, 1 (2013)
42. S. Hamada, S. Hibarino, K. Ikeue, M. Machida, Appl. Catal. B Environ. **74**, 197 (2007)
43. S.H. Sarijo, S.A.I.S.M. Ghazali, M.Z. Hussein, A.H. Ahmad, Mater. Today Proc. **2**, 345 (2015)
44. M. Z. Bin Hussein, A. H. Yahaya, Z. Zainal, L. H. Kian, Sci. Technol. Adv. Mater. **6**, 956 (2005).
45. P. S. Braterman, Z. P. Xu, F. Yarberry, in *Handb. Layer. Mater.*, edited by S. M. Auerbach, K. A. Carrado, P. K. Dutt (Marcel Dekker, New York, 2004), p. 647.
46. S. Li, Y. Shen, M. Xiao, D. Liu, L. Fan, Arab. J. Chem. (2015). https://doi.org/10.1016/j.arabjc.2015.04.034
47. S.F. Hosseini, M. Zandi, M. Rezaei, F. Farahmandghavi, Carbohydr. Polym. **95**, 50 (2013)
48. M.Z. Hussein, N.S.S.A. Rahman, S.H. Sarijo, Z. Zainal, Appl. Clay Sci. **58**, 60 (2012)
49. Y.S. Ho, G. Mckay, Process Biochem. **34**, 451 (1999)
50. T. Kodama, Y. Harada, M. Ueda, K.I. Shimizu, K. Shuto, S. Komarneni, Langmuir **17**, 4881 (2001)
51. P.L. Ritger, N.A. Peppas, J. Control. Release **5**, 37 (1987)
52. E.P. Holowka, S.K. Bhatia, *Drug Delivery: Materials Design and Clinical Perspective* (Springer, New York, 2014)
53. N. Hashim, Z. Muda, S.A. Hamid, I.M. Isa, A. Kamari, A. Mohamed, M.Z. Hussein, S.A. Ghani, J. Phys. Chem. Sci. **1**, 1 (2014)